Performance of the Generalized Multipole Technique (GMT/ MMP) in Antenna Design and Optimization

Roger Yew-Siow Tay
Florida Corporate Electromagnetics Research Laboratory
MOTOROLA, USA
and
Niels Kuster
Laboratory of Electromagnetic Fields and Microwave Electronics
Swiss Federal Institute of Technology
Zurich, SWITZERLAND

Abstract

During the last decade, the generalized multipole technique (GMT) has been extensively studied, improved and applied to many electromagnetics problems such as bioelectromagnetics, optics, waveguides and electromagnetic compatibility (EMC), but little has been reported towards utilizing this method for antenna design and optimization. On the other hand, the few published examples of simple dipoles and helices in the close vicinity of lossy scatterers have suggested the potential significance of GMT for antenna design purposes. In this paper, the applicability of the GMT based 3D multiple multipole (3D MMP) code for simulation of wire antennas has been investigated.

To evaluate the advantages and limitations of 3D MMP, several basic types of wire antenna configurations were simulated. These were linear and linear array, helical, and physically constrained low profile antennas. To validate the method's performance, we calculated radiation patterns, impedance, return loss, reflection coefficient, VSWR, and compared them to available results from experiments and/or results published by others using different techniques.

This investigation showed several conceptual advantages of this technique for antenna simulations. Furthermore, the thin-wire expansion in combination with multipoles and roof top functions provides a great degree of flexibility in modeling. The most recently implemented expansion, "line multipoles," extends the code's efficiency to non-thin-wire configurations (e.g., helix with small ratio of pitch to wire diameter).

Critical issues of modeling are the feedpoint and wire tip area, matching point locations and segment length-to-diameter ratio. Symmetries are used where possible to minimize computation time without loss of generality as any antenna element may easily be assembled in non-symmetrical configurations with the block-iterative solver. In order to achieve better confidence on more complex configurations, extensive studies were performed to increase efficiency and stability of modeling and will be discussed. In addition, the numerical validation techniques were extended to satisfy the special requirements of antenna simulations.

These studies demonstrate the potential of GMT/ MMP for use in analysis, synthesis and optimization of antennas.

1.0 Introduction

Several techniques have been developed and are being applied to analyze antennas embedded in a given environment. In general, these techniques can be classified as experimental, analytical, and numerical.

Analytical techniques are limited to simple geometries and can therefore only be applied to a narrow range of practical problems. In addition, quite a high degree of ingenuity, experience, and effort are required to apply them.

Despite the fact that they are expensive and time consuming, experimental techniques still continue to be the most widespread approach for synthesis, analysis and optimization of antennas. They do not usually allow much flexibility in parameter variation.

Various numerical techniques have been developed during the last three decades to solve EM scattering problems in general and antenna problems in particular. Nevertheless, computer aided design (CAD) tools for antenna optimizations are not widely used in development. The reasons are that none of the currently applied codes based on FDTD, FE and MoM techniques fully meet the basic requirements, which are: ease of use, high accuracy and efficient techniques for numerical validation. On the other hand, as in other areas of engineering, good CAD tools should offer low cost, high efficiency and qualitatively improved physical insight, which would significantly accelerate the development of new designs.

The GMT based 3D MMP code offers various features favoring antenna simulations. However, little has been reported about the utilization of this method for antenna design and optimization. Only a few published examples of simple dipoles and helices in the close vicinity of lossy scatterers [Kuster, 1992] have suggested the potential significance of GMT for antenna design pur-

poses. It is the aim of this paper to evaluate the potential of this technique as a CAD tool for antennas.

2.0 GMT / 3D MMP code

Since this is a special issue for GMT, and many excellent papers and books discussing the theory of GMT and its 3D MMP implementation have been published, a detailed introduction is omitted here. Readers are advised to refer to [Hafner, 1990; Hafner & Bomholt, 1993] for a complete discussion of the technique and to [Kuster, 1993] for a description of simulation and solution validation techniques.

However, the conceptual advantages of GMT pertaining to antenna simulation are briefly discussed in the following.

The 3D MMP code provides various expansion functions all of which are analytical solutions of the time harmonic homogeneous Maxwell equations. The most important sets of expansion functions are point and line multipoles as well as roof top functions. Geometrically based tools support the user in selecting the set of functions that most efficiently approximate the unknown fields. In doing so, it can be ensured that the pole of the functions is located as far as possible from the boundaries. The parameters are determined by approximating the boundary conditions in the sense of least squares, whereas the weights of the equations are based on the energy concept.

This approach reveals some important conceptual advantages, valid in general and for antenna simulations in particular. 1) The concept is based on the definition of an error, which is minimized, which greatly facilitates numerical validation. Furthermore, as GMT is a boundary technique, the problem of solution validation is reduced by one dimension. 2) A great degree of independence between structure dimensions and wavelength is achieved. 3) The fields in all closed and open subdomains are always exact Maxwell fields in any homogeneous, linear and isotropic materials. 4) The implemented pole expansion functions are well suited to modeling radiating structures. 5) Since the errors in meeting the boundary conditions are uniformly distributed on the boundaries, the integral values within the accuracy of the achieved solution can be computed in the near as well as in the far field without any special considerations. 6) Interaction with the environment (e.g., human head in the extreme vicinity of the antenna) can conveniently be solved by the block-iterative solver [Kuster and Bomholt, 1994] without losing accuracy and even more importantly, without multiplying the scale of the numerical problem. 7) The ongoing work of coupling MMP with finite element (FE) techniques [Bomholt, 1994] will further broaden the suitability of the code, especially with respect to simulating the environment (e.g., inhomogeneous scatterers).

Furthermore, the code is supported by high level graphical interfaces for general purposes.

3.0 Simulations

3.1 Modeling

Point multipoles are the most flexible expansion functions. However, in the case of long structures such as wires, the large number of point multipoles required resulted in poor efficiency [Kuster & Ballisti, 1989]. To overcome this problem, the thin wire expansion used by NEC was adopted and implemented in 1990 [Leuchtmann & Bomholt, 1990]. As the prerequisites for the thin wire approximation were not met for all antenna configurations, the *line multipole* expansion [Leuchtmann & Gnos, 1994] was developed and recently implemented. The thin wire approximation corresponds to the zero order term of the line multipole.

The optimal locations previously found for matching points on wires [Leuchtmann, 1991] have proven to be an excellent choice for the antenna configurations tested. As all test cases met the requirements for the thin wire approximation, all simulations were performed with an axially symmetrical current distribution on the wires. In addition, symmetries were used where possible.

The feedpoint gap was expected to be the most critical area for modeling. However, accurate modeling of the feedpoint area, which could be quite tedious, is not required for thin structures. Extensive tests have shown that a suitable and simple approach is one in which the first wire element is the current driving source and the boundary conditions are enforced only from the middle of the second wire element. A stable solution is accomplished by introducing special weights for the first few matching points. Any errors introduced in the E-field due to this rather coarse modeling have proven to be highly local (quasi static) and are easily by-passed by selecting integral paths that avoid the closest vicinity of these first matching points.

The modeling of the antenna tips has been shown to be more critical than that of the feedpoint area. For antenna diameters that are greater than 0.015λ an accurate modelling of the tips by using point multipoles in addition to the line multipoles is required.

Maintaining proper ratio of the wire element length to the wire diameter is also critical to ensure accurate results.

3.2 Numerical Validation

All the simulated results were validated with the procedures described in [Kuster, 1993]. This basically consists of 1) the evaluation of the error distribution satisfying the boundary conditions, 2) the checking of the solution stability (feed point impedance, radiation pattern, total power radiated) by expanding the fields with different expansions, by different matching point distributions and by scanning over a broad frequency range, 3) the checking of other requirements such as the comparison of feed point impedance and radiated power. 4) In addition, all results are qualitatively checked by animated visualization of electric, magnetic and Poynting vector fields.

4.0 Measurements

Whenever possible, the solutions are compared with data available from literature obtained either by measurements, analytical approximations or numerical simulations. For the cases where no data was available, measurements were conducted.

The setup for the impedance characterization of antennas is conceptually quite simple and straightforward. In practice, the cable used and the surrounding environment have tremendous impact on the measurement. Calibration of the measurement setup is extremely important especially at higher frequencies. If the electrical delay is not properly compensated for the choice of connector used at the feedpoint, then phase errors will occur. Hence, both the real and imaginary part of the input impedance will be incorrect. Fig. 1 shows the setup that was used in our experiment. The ground plane used in this experiment was a 3 foot square copper-plated printed circuit board which was placed at least 5 feet away from the nearest object. The equipment used in the setup includes an HP8753C Network Analyzer, HP85047A S-parameter Test Set, and an IBM-compatible PC for data acquisition, when necessary.

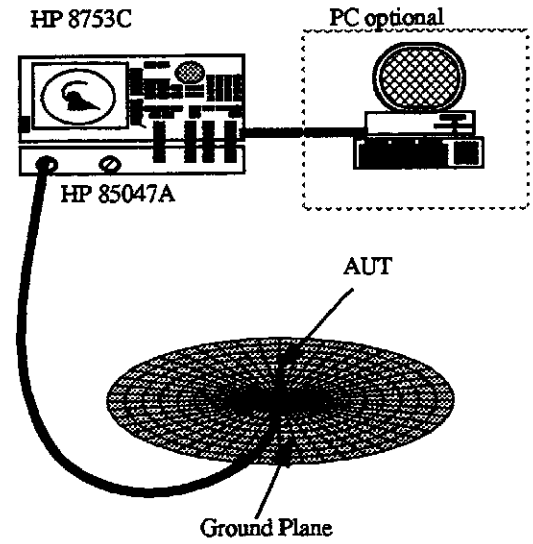

Fig. 1. Setup for antenna impedance measurement.

5.0 Results

The basic theories concerning antennas can be found in many excellent text books and papers. Hence, we make no attempt to cover them in this paper. However, a couple of the definitions used are reiterated in the following.

Considering the antenna impedance as $Z_a = R_a + jX_a$ and the characteristic impedance of the transmission line feeding the antenna as Z_0, then the voltage reflection coefficient ρ is

$$\rho = \frac{Z_a - Z_0}{Z_a + Z_0} \qquad \text{(EQ 1)}$$

The *VSWR* is related to ρ by

$$VSWR = \frac{1 + |\rho|}{1 - |\rho|} \qquad \text{(EQ 2)}$$

We also treat the input resistance R_{in} as

$$R_{in} = R_{rad} + R_s \qquad \text{(EQ 3)}$$

where R_{rad} is the radiation resistance, and R_s is the loss resistance at the corresponding frequency. R_s is only considered for the experimental results as perfectly conductive wires are used for the numerical models. The input impedance is calculated by the integrated value of the complex E-field vector across the feeding gap divided by

the complex current value. From the parameters given above, one can determine the efficiency, return loss and any other means of presenting the data convenient to antenna engineers. External graphical interfaces were used to present the figures in this paper.

To compare our results with King-Middleton data, the same definition of Ω as appeared in the King-Middleton approximation [King, 1965] has been used

$$\Omega = 2 \times ln(\frac{2h}{a}) \qquad \text{(EQ 4)}$$

where a is the radius of the antenna and h is the half height of the dipole.

5.1 Straight Dipole

The dipole antenna is the simplest and one of the most widely used antennas. Excellent discussions of this subject can be found in many texts, e.g., in [King, 1965]. The first tests conducted were on different dipoles, two of which are documented here. All results were compared with those of King-Middleton second order expansion. Fig. 2 shows the geometry of a simple dipole.

Figs. 3 and 4 show the comparison of input impedance for two dipole antennas computed with MMP code, and the King-Middleton second-order expansion for Ω equal to 10 and 15 respectively. Both figures show excellent agreement between the two sets of data except when the frequencies are several times higher than the resonant frequency for the case of Ω=10. These differences are at least partly explained by the different shapes of the antenna tips which is a half sphere in case of the MMP modeling whereas King-Middleton used a flat tip. It is obvious that the effects due to such differences increase with radius and frequency.

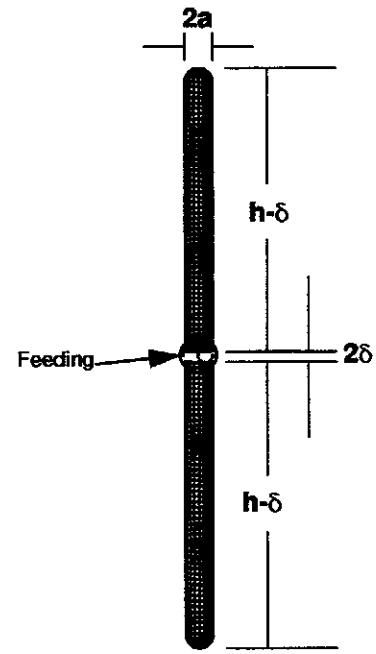

Fig. 2. A simple dipole.

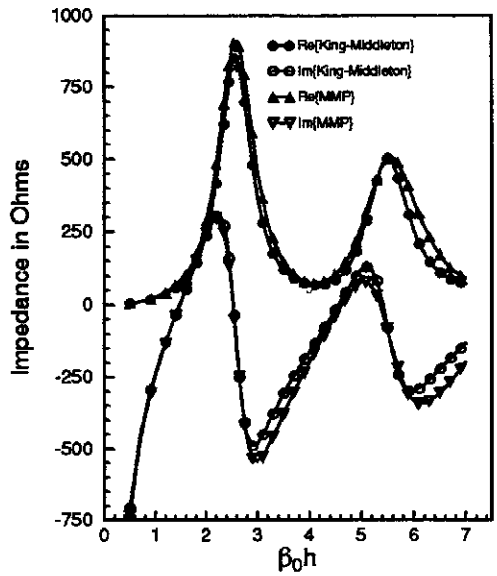

Fig. 3. Comparison of input impedance computed by MMP, and King-Middleton data for Ω=10.

5.2 Yagi-Uda Array

The next more complicated configuration is the Yagi-Uda Array, with which the performance for coupled excited and passive antenna elements can be tested.

Fig. 5 shows a general description of the Yagi-Uda parameters used in this paper. As a test case, a 27-element array was simulated and compared to the results published by Thiele using the method of moment (MoM) [Thiele, 1969]. The parameters are:

L_d = 0.406 λ
L_e = 0.47 λ
L_r = 0.50 λ
d_r = -0.125 λ

d_d = 0.34 λ
Number of directors = 25
Radius of element = 0.003 λ

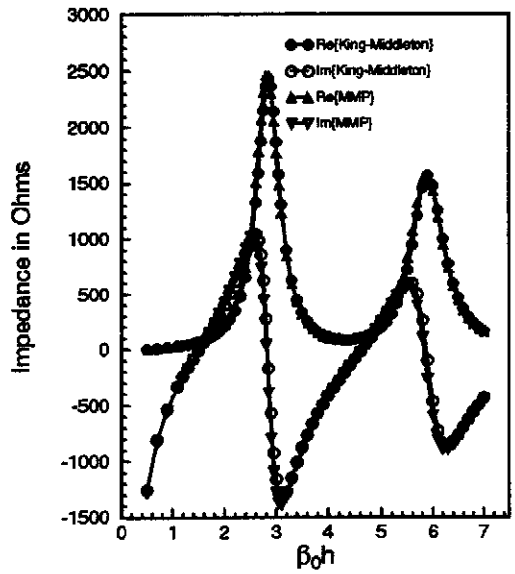

Fig. 4. Comparison of input impedance computed by MMP, and King-Middleton data for Ω=15.

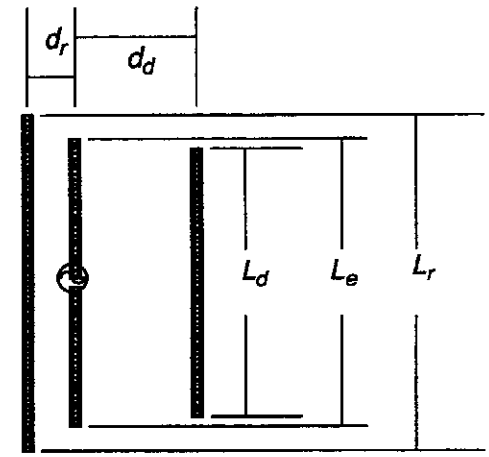

Fig. 5. General configuration of a Yagi-Uda array.

Fig. 6 shows the current amplitude calculated at the center of each element for all the elements, and then normalized to the excitation of the array. These data were compared with published data using MoM. Director numbers = -1,0,1,2... shown in the x-axis, are the reflector, exciter and the directors from the exciter. The results show good agreement except for the last few elements of the directors. However, measurement to determine which solution is more accurate is very difficult and laborious. We make no attempt to validate them at this time.

To further illustrate, we computed another 8-element Yagi-Uda array using dimensions from other published results [Thiele, 1969]. This 8-element array has the following dimensions:

L_d = 0.405 λ
L_e = 0.47 λ
L_r = 0.50 λ
d_r = -0.125 λ
d_d = 0.34 λ
Number of directors = 6
Radius of element = 0.003 λ

Fig. 7 and 8 show the radiation plot of average Poynting vector. It is interesting to note that it exhibits more and a higher level of the side lobes in the H-plane than in the E-plane. Our radiation pattern shows generally good agreement with Thiele's results in the forward direction and in most of the side lobes except that our results show a tiny lobe in the backward direction.

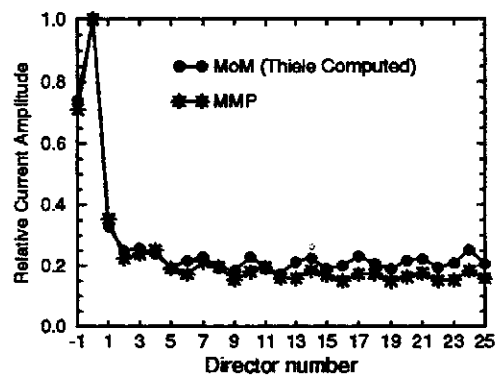

Fig. 6. Relative current amplitude comparison computed using MMP, and MoM for 27-element Yagi-Uda array.

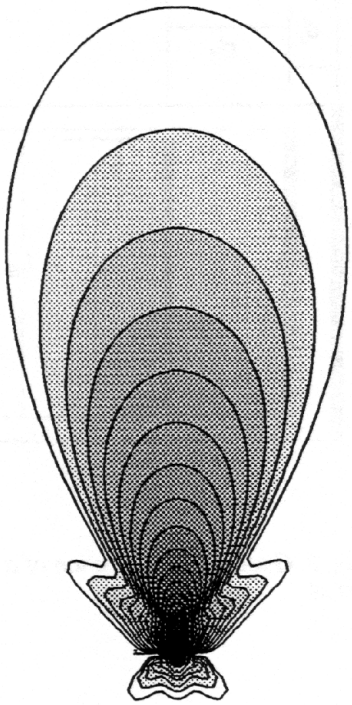

Fig. 7. E-plane radiation pattern of an 8-element Yagi-Uda array.

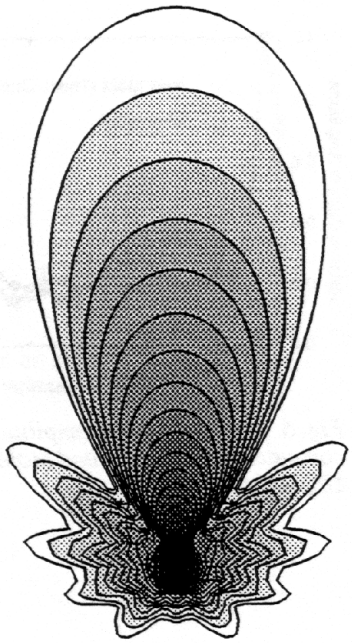

Fig. 8. H-plane radiation pattern of an 8-element Yagi-Uda array.

5.3 Axial Mode Helical Antennas

The geometry of helical antennas is shown in Fig. 9. In most cases the helix is used with a ground plane. Some of the essential parameters to describe the physical dimensions of a helix are:

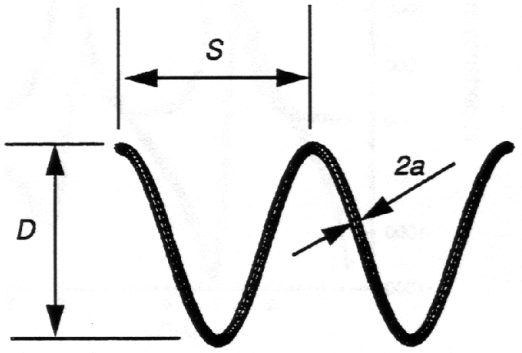

Fig. 9. Helix and its associated dimensions.

D = diameter of helix (center to center)
S = spacing between turns (center to center)
C = circumference of helix = πD
L = length of 1 turn = $\sqrt{(S^2 + C^2)}$
α = pitch angle = $\tan^{-1} \frac{S}{\pi \cdot D}$
n = number of turns
a = radius of wire
h = height or length of helix

Axial mode or endfire mode helices (i.e., C comparable to or greater than its operating wavelength; S relatively large), generally have extremely broad operating bandwidths and elliptic (with low ellipticity) to circular polarization [Kraus, 1948 & 1988]. Increasing the number of turns will increase directivity but decrease radiation beamwidth.

Fig. 10 shows the computed radiation pattern of a helix operating in axial mode (C_λ=0.70153) with the following helical dimensions:

Number of turns $n = 5$
Diameter of helix D = 46.52 mm
Radius of wire a = 0.74 mm
Height of helix h = 163 mm
Pitch angle α = 16.40°
Gap between helix and ground plane = 10 mm
Wavelength λ = 0.20833 m
Circumference C =0.14615 m
$C_\lambda = C/\lambda$ = 0.70153

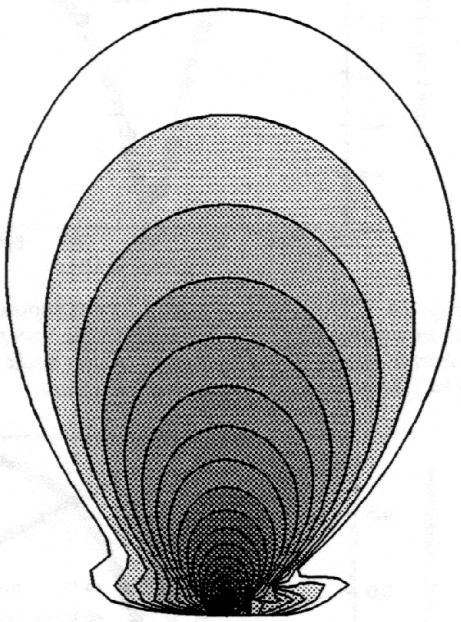

Fig. 10. Radiation pattern of a helical antenna operating in axial or end-fire mode.

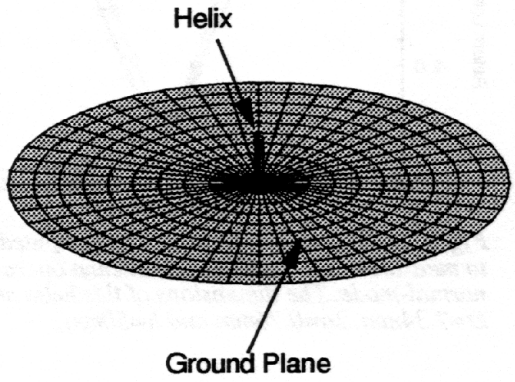

Fig. 11. Helix mounted on ground plane operating in normal mode.

5.4 Normal Mode Helical Antennas

In contrast to axial mode antennas, helices radiating in the direction normal to the axis typically have more turns and much smaller diameters with respect to wavelength. Fig. 11 shows a geometrical representation of a normal-mode helical radiator, this set-up includes a helix whose diameter $D << \lambda$ and $h < \lambda$. The helix is excited by connecting one end to the center conductor of a coaxial cable, with the outer conductor of the cable connected to the ground plane. For this test case, two helices are built and measured with the dimensions:

	Helix #1	Helix #2
n =	10	10
D =	7.34 mm	7.34 mm
a =	0.38 mm	0.38 mm
h =	50 mm	100 mm

A common radiation pattern of a normal-mode helical dipole is shown in fig. 12. This radiation pattern was computed with the dimensions of helix #2 for λ=0.773m and C_λ=0.0298. Figs. 13-15 were computed with the dimension of helix #1 and figs. 16-18 were computed with the dimension of helix #2. The computed results have a slight frequency shift. One explanation could be that the helical structure generated for computation has a slightly smaller diameter than the actual helix. These helices were simulated by choosing thin wire expansion as the basis functions. The helix was constructed with short and straight segments joined together. In this experiment, 8 segments per turn were used and were inscribed. In general, the agreement of both were within the uncertainties of the experimental setup.

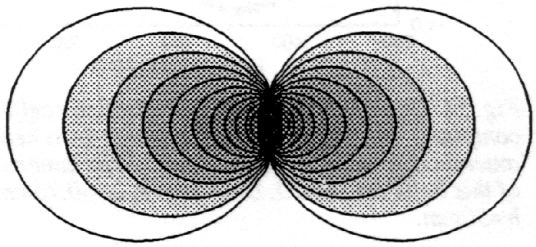

Fig. 12. Plot of radiation pattern for a helical antenna operating in normal-mode.

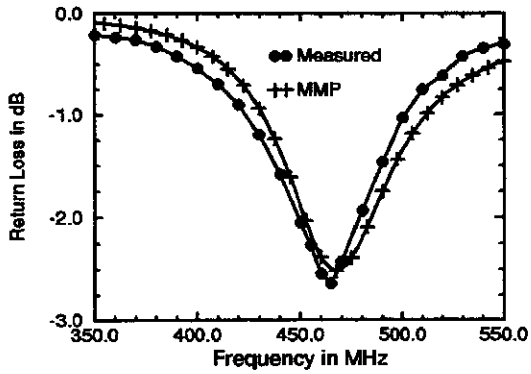

Fig. 13. Comparison of return loss computed with MMP to measurements for a helical antenna operating in normal-mode. The dimensions of this helix are: n=10, D=7.34mm, 2a=0.76mm and h=50mm.

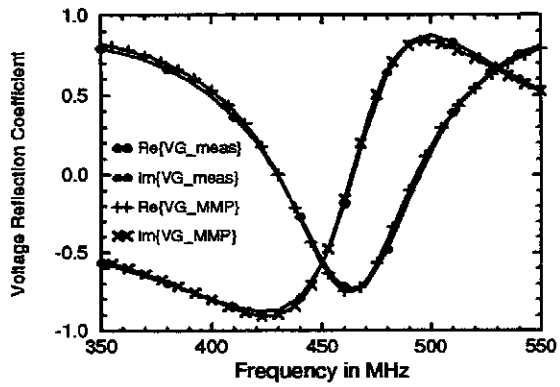

Fig. 14. Comparison of voltage reflection coefficient computed with MMP to measurements for a helical antenna operating in normal-mode. The dimensions of this helix are: n=10, D=7.34mm, 2a=0.76mm and h=50mm.

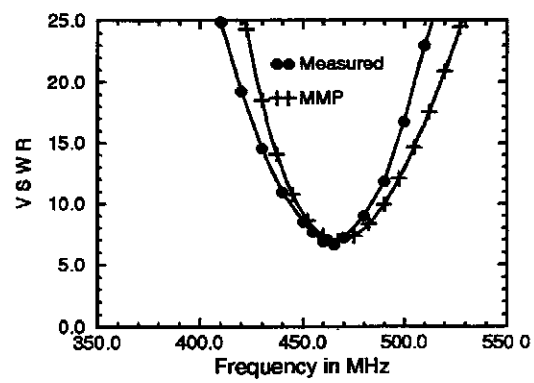

Fig. 15. Comparison of VSWR computed with MMP to measurements for a helical antenna operating in normal-mode. The dimensions of this helix are: n=10, D=7.34mm, 2a=0.76mm and h=50mm.

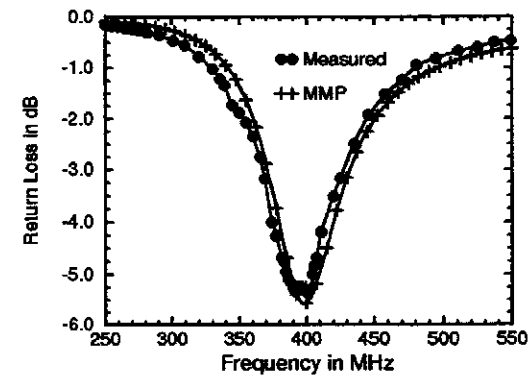

Fig. 16. Comparison of return loss computed with MMP to measurements for a helical antenna operating in normal-mode. The dimensions of this helix are: n=10, D=7.34mm, 2a=0.76mm and h=100mm.

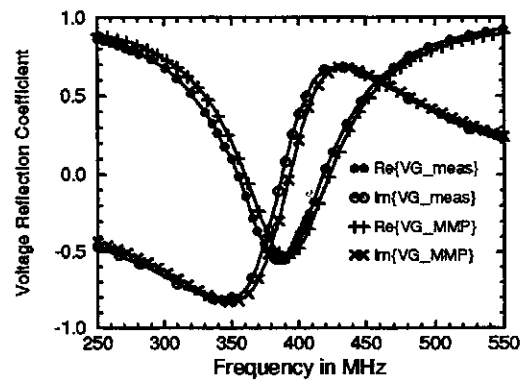

Fig. 17. Comparison of voltage reflection coefficient computed with MMP to measurements for a helical antenna operating in normal-mode. The dimensions of this helix are: n=10, D=7.34mm, 2a=0.76mm and h=100mm.

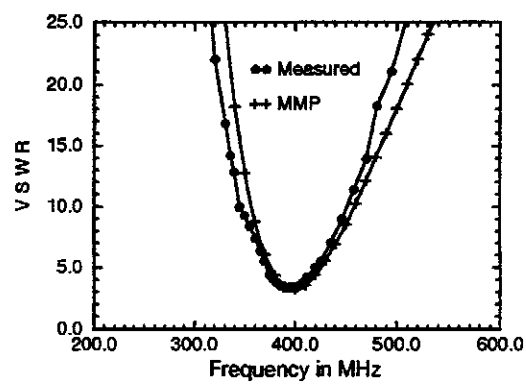

Fig. 18. Comparison of VSWR computed with MMP to measurements for a helical antenna operating in normal-mode. The dimensions of this helix are: n=10, D=7.34mm, 2a=0.76mm and h=100mm.

5.5 Inverted-L (ILA) Configuration

The last test case is the Inverted-L or ILA configuration. An Inverted-L antenna configuration is shown in fig. 19. In this configuration, $h < \lambda_0/4$ and f_0 varies with h for a given length $l+h$ of wire.

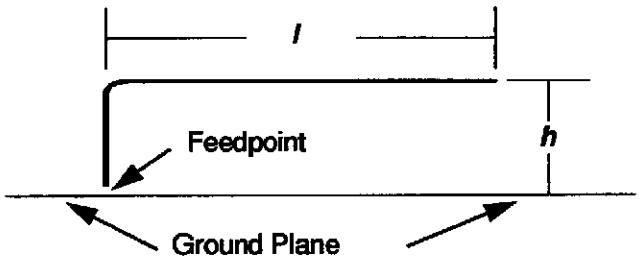

Fig. 19. An Inverted-L configuration.

Fig. 20-22 show comparisons of impedance characteristics between computed and measured results for an ILA antenna of the following dimensions:

h = 65 mm
l = 80 mm
2a = 1.48 mm

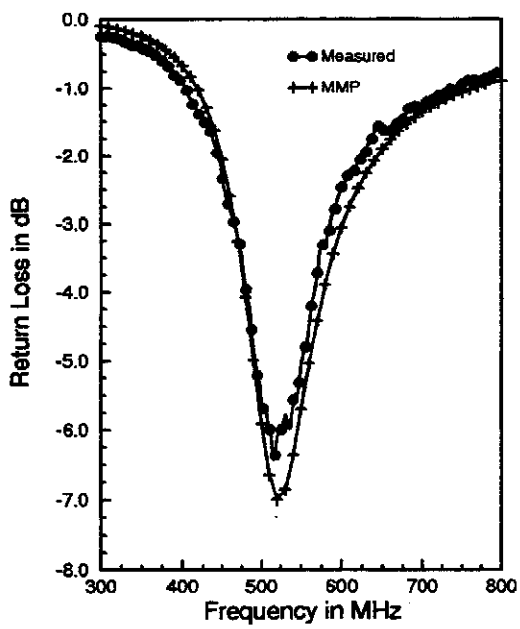

Fig. 20. Comparison of return loss computed with MMP to measurements for an Inverted-L wire antenna of l=80mm, h=65mm and 2a=1.48mm.

These plots show close correlation between measurement and simulation, even for $d\Omega/d\omega$, where Ω is the reactance of the input admittance and ω is the angular frequency. Fig. 23 shows the computed return loss versus frequency plot of varying height h by keeping everything else constant. From the plot, the resonant frequency increases with decreasing height h and the return loss improves with increasing height.

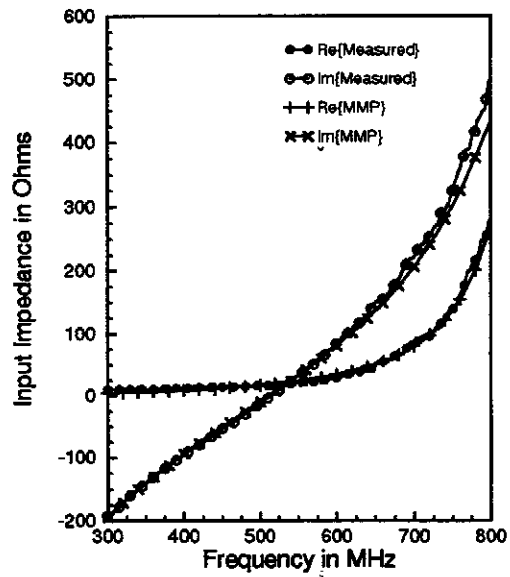

Fig. 21. Comparison of input impedance computed with MMP to measurements for an Inverted-L wire antenna of l=80mm, h=65mm and 2a=1.48mm.

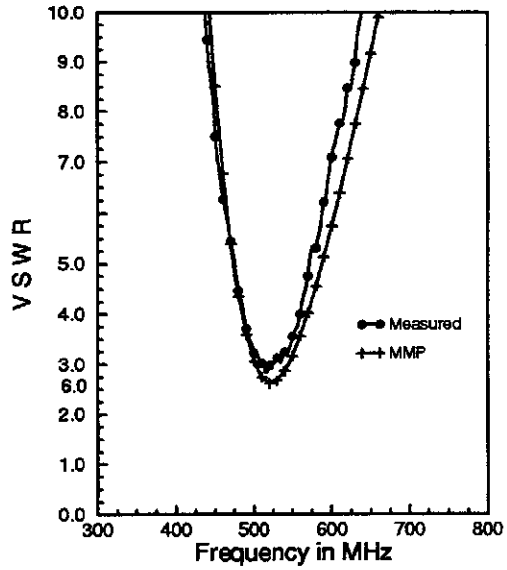

Fig. 22. Comparison of VSWR computed with MMP to measurement for an Inverted_L wire antenna of l=80mm, h=65mm and 2a=1.48mm.

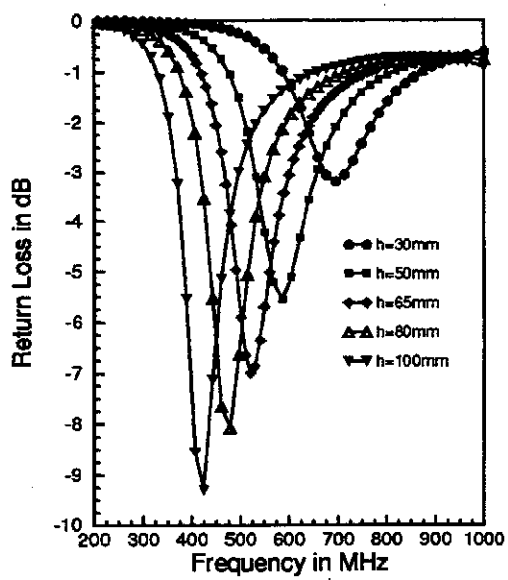

Fig. 23. Return loss of Inverted_L wire antennas computed with MMP for l=80mm, 2a=1.48mm and varying h of 30, 50, 65, 80 and 100mm.

6.0 Conclusions

All results are in good to excellent agreement with measured or otherwise published data. Explanations for the various differences could not be provided in all cases, especially as the published data does not quantify uncertainties of the computed or measured values. Although the range of uncertainty can be assessed by 3D MMP for other types of problems [Kuster & Balzano, 1992, Kuster, 1993], such an assessment was not possible in this case. This is mainly due to the problem of possible error propagation along the wires. However, assessments of the uncertainties should now become possible by the recently implemented line multipoles which enforce current continuity even along curved wires.

In conclusion, these studies have revealed the excellent potential of 3D MMP for antenna simulations. This has encouraged us to start a project to develop a specific CAD tool based on 3D MMP for analysis, synthesis and design of antennas.

7.0 Acknowledgments

The help and comments of Ray Ballisti, Lars Bomholt, Oscar Garay, Pascal Leuchtmann, Thomas Manning and Peter Regli are greatly appreciated.

References

[1] Bomholt, H.L., "Coupling of the Generalized Multipole Technique and Finite Element Method," ***in this issue***.

[2] Hafner, C., "The Generalized Multipole Technique for Computational Electromagnetics," Artech House, Inc., Boston, 1990.

[3] Hafner, C. and Bomholt, L. H., "The 3D Electrodynamic Wave Simulator," John Wiley & Sons, 1993

[4] King, R. W. P., "The Theory of Linear Antennas," Harvard University Press, 1965.

[5] Kraus, J. D., "Antennas," McGraw-Hill, 2nd. edition, 1988.

[6] Kraus, J. D. "Helical Beam Antennas for Wide-Band Applications," ***Proceedings of The I.R.E.***, Vol. 36, pp. 1236-1242, October 1948.

[7] Kuster, N. and Ballisti, R., "MMP-Method Simulation of Antennae with Scattering Objects in the Closer Near Field," ***IEEE Transactions on Magnetics***, Vol. 25, pp. 2881-2883, July 1989

[8] Kuster, N., and Balzano, Q., "Energy Absorption Mechanism by Biological Bodies in the Near Field of Dipole Antennas Above 300 MHz," ***IEEE Trans. on Vehicular Technology***, Vol. 41, No. 1, February 1992.

[9] Kuster, N., "Multiple Multipole Method Applied to an Exposure Safety Study", in ***ACES Special Issues on Bioelectromagnetic Computations***, vol. 7, pp. 43-60, Fleming, A. and Joyner, K. H. Eds. Applied Electromagnetics Society, 1992.

[10] Kuster, N., "Multiple Multipole Method for Simulating EM Problems Involving Biological Bodies," ***IEEE Transactions on Biomedical Engineering***, Vol. 40, pp. 611-620, July 1993.

[11] Kuster, N., and Bomholt, L. H., "A Block Iterative Technique to Expand MMP's Applicability to EM Problems of Higher Complexity" ***IEEE Transactions on Microwave Theory and Techniques***, Vol. 42, pp. 875-883, May 1994

[12] Leuchtmann, P. and Bomholt, L. H., "Thin Wire Feature for the MMP Code," in ***6th Annual Review of Progress in Applied Computational Electromagnetics (ACES), Conference Proceedings***, Monterey, March 1990.

[13] Leuchtmann, P., "Optimal Locations for Matching Points for Wire Modelling with MMP," ***Applied Computational Electromagnetics Society (ACES) Journal***, Vol. 6., pp. 21-37, Dec. 1991.

[14] Leuchtmann, P. and Gnos, M., "Curved Line Multipoles for the MMP-Code," ***in this issue***.

[15] Thiele, G. A., "Analysis of Yagi-Uda-Type Antennas," ***IEEE Trans. Antennas and Propagation***, Vol. AP-17, pp. 24-31, January 1969.